Graphene-Based Artificial Synapses with Tunable Plasticity

Wang, He; Laurenciu, Nicoleta Cucu; Jiang, Yande; Cotofana, Sorin

DOI
10.1145/3447778

Publication date
2021

Document Version
Final published version

Published in
ACM Journal on Emerging Technologies in Computing Systems

Graphene-Based Artificial Synapses with Tunable Plasticity

HE WANG, NICOLETA CUCU LAURENCIU, YANDE JIANG, and SORIN COTOFANA,
Computer Engineering Laboratory, Delft University of Technology, The Netherlands

Design and implementation of artificial neuromorphic systems able to provide brain akin computation and/or bio-compatible interfacing ability are crucial for understanding the human brain's complex functionality and unleashing brain-inspired computation's full potential. To this end, the realization of energy-efficient, low-area, and bio-compatible artificial synapses, which sustain the signal transmission between neurons, is of particular interest for any large-scale neuromorphic system. Graphene is a prime candidate material with excellent electronic properties, atomic dimensions, and low-energy envelope perspectives, which was already proven effective for logic gates implementations. Furthermore, distinct from any other materials used in current artificial synapse implementations, graphene is biocompatible, which offers perspectives for neural interfaces. In view of this, we investigate the feasibility of graphene-based synapses to emulate various synaptic plasticity behaviors and look into their potential area and energy consumption for large-scale implementations. In this article, we propose a generic graphene-based synapse structure, which can emulate the fundamental synaptic functionalities, i.e., **Spike-Timing-Dependent Plasticity (STDP)** and **Long-Term Plasticity**. Additionally, the graphene synapse is programable by means of back-gate bias voltage and can exhibit both excitatory or inhibitory behavior. We investigate its capability to obtain different potentiation/depression time scale for STDP with identical synaptic weight change amplitude when the input spike duration varies. Our simulation results, for various synaptic plasticities, indicate that a maximum 30% synaptic weight change and potentiation/depression time scale range from [−1.5 ms, 1.1 ms] to [−32.2 ms, 24.1 ms] are achievable. We further explore the effect of our proposal at the **Spiking Neural Network (SNN)** level by performing NEST-based simulations of a small SNN implemented with 5 leaky-integrate-and-fire neurons connected via graphene-based synapses. Our experiments indicate that the number of SNN firing events exhibits a strong connection with the synaptic plasticity type, and monotonously varies with respect to the input spike frequency. Moreover, for graphene-based Hebbian STDP and spike duration of 20 ms we obtain an SNN behavior relatively similar with the one provided by the same SNN with biological STDP. The proposed graphene-based synapse requires a small area (max. 30 nm^2), operates at low voltage (200 mV), and can emulate various plasticity types, which makes it an outstanding candidate for implementing large-scale brain-inspired computation systems.

CCS Concepts: • **Hardware → Neural systems**; **Emerging technologies;**

Additional Key Words and Phrases: Artificial synapse, graphene, neuromorphic computing, synaptic plasticity, STDP, LTP, LTD

This is an extended version of the original conference paper, "Graphene Nanoribbon-based Synapses with Versatile Plasticity", which appeared in NANOARCH 2019.

Authors' address: H. Wang, N. Cucu Laurenciu, Y. Jiang, and S. Cotofana, Computer Engineering Laboratory, Delft University of Technology, Delft, The Netherlands; emails: {H.Wang-13, N.Cuculaurenciu, Yande.Jiang, S.D.Cotofana}@tudelft.nl.

1550-4832/2021/06-ART50 $15.00
https://doi.org/10.1145/3447778

ACM Reference format:
He Wang, Nicoleta Cucu Laurenciu, Yande Jiang, and Sorin Cotofana. 2021. Graphene-Based Artificial Synapses with Tunable Plasticity. *J. Emerg. Technol. Comput. Syst.* 17, 4, Article 50 (June 2021), 21 pages.
https://doi.org/10.1145/3447778

1 INTRODUCTION

The human brain is a high performance natural computation system, which comprises billions of neurons and trillions of synapses. Its unique and attractive properties, e.g., energy efficiency, real-time reaction, robustness, suitability for complex task solving and highly parallel information processing ability, spurred the development of a disruptive computing paradigm, **the Neuromorphic Computing (NC)** [35]. In the past decades many efforts have been made to develop brain-inspired computation paradigms [15, 25, 29, 30] and biologically inspired neuromorphic systems [1, 8, 14, 37] based on artificial neurons and synapses. The development of NC promoted research aiming at understanding the brain's fundamental operational principles and achieving human-brain-comparable computation ability.

The synapse, which is the most abundant components in neural systems, is a junction connecting two neurons and sustaining the information transmission between them. The synaptic transmission efficiency is variable and appears as the potentiation or depression of the transmitted signals [10, 20]. The synaptic transmission efficiency strengthening or weakening is known as synaptic plasticity, which is believed to be the basis of learning and memory in human brain. From synaptic behavior point of view, an artificial synapse ought to implement two basic functionalities: (i) **Spike-Timing-Dependent Plasticity (STDP)**, which changes the transmission efficiency depending on the relative timing difference between the pre-synaptic and post-synaptic spikes [11], and (ii) Long-Term Plasticity in its two flavours, i.e., **Long-Term Potentiation (LTP)** and **Long-Term Depression (LTD)**, which is a persistent synaptic transmission efficiency change [5].

Since there are trillions of synapses in the nervous system that are essential for supporting the human brain complex functionality, designing and implementing artificial synapses for any large-scale biological-inspired computation systems received massive attention. In most state-of-the-art neuromorphic systems, the artificial synapses are implemented with complex CMOS circuitry [6, 19, 36, 39]. However, as CMOS scaling is approaching atomic feature size, which results in high power consumption and low reliability, CMOS-based synapses bring limitations to scalability, energy efficiency, and integration density of large-scale neuromorphic systems. Besides, CMOS-based artificial synapses cannot efficiently mimic the analog synaptic behavior. Recently, emerging resistive switching memory devices [43] attracted interest and have been used to implement artificial synapses [4, 27, 32, 38]. The obtained artificial synapses exhibit outstanding properties, e.g., inherently analog behavior, simple structure (one single or a few resistive switching memory devices for one synapse), and good scalability potential. However, they suffer from temporal and spatial variability of the resistive states and undesired stochastic behavior, which may cause neuromorphic system instability. They also need to be operated at relatively high voltage, which precludes the implementation of energy-efficient computation systems.

Graphene, a two-dimensional carbon atom honeycomb lattice, has lately emerged as one of the most prominent post-Si forerunners, as it exhibits a wealth of outstanding properties, e.g., low power consumption, ballistic transport, ultimate thinness, inherently analog nature, and biocompatibility [2, 3, 17]. Due to its unique properties, graphene-based devices have been utilized for Boolean logic gate implementations [26, 33, 42]. Moreover, previous work on graphene-based synapses demonstrated that graphene-based devices can emulate synaptic plasticity. In [44], the authors demonstrated various synaptic plasticities, however, their proposed artificial synapses

operate with quite large back-gate voltage (20 V, 40 V) and input signals (2 V), which makes them power hungry and inappropriate for energy-effective implementations. Moreover, the obtained synaptic transmission efficiency change is extremely small ($< 0.01\%$) and only restricted synaptic plasticity types are provided. In [41], a graphene-based synapse is proposed that relies on changing the Li ion concentration between graphene layers to control the device conductance. This synapse endows low-power switching ability, low variability, and is potentially suitable for large-scale implementations. However the reported conductance change is small ($< 2\%$) and the considered spikes timing difference around 1000 ms is significantly different from the one observed in natural synapses (≈ 80 ms).

In this article, we propose a generic graphene-based artificial synapse structure, which consists of a single-layer Graphene Nanoribbon (GNR) on top of an insulating material with a doped substrate serving as a back-gate. The current flow in the GNR channel is induced by applying a drain-to-source bias voltage. The synaptic transmission efficiency, which is reflected as the conductance of the proposed synapses, can be modulated by means of external voltages, e.g., via two top-gates and one back-gate. To mimic the synaptic behavior, we consider two fundamental synapse functionalities, i.e., STDP and Long-Term Plasticity. By carving the GNR geometries and contact topologies of the proposed structure, we successfully obtain various synaptic plasticity, including balanced Hebbian STDP, potentiation biased anti-Hebbian STDP, balanced anti-Hebbian STDP, potentiation biased anti-Hebbian STDP, Long-Term Potentiation, and LTD. We also demonstrate that the same device can emulate both excitatory and inhibitory synaptic behaviors by simply changing the back-gate voltage. The GNR device is biased at 0.2 V and operates on 110 mV inputs, which is consistent with measured biological synapses data and makes it operation compatible with natural neural matter. Besides, by applying input spikes with different spike duration, the proposed synapses can emulate STDP with varying potentiation/depression time scale without affecting the obtained amplitude of the synaptic transmission efficiency change. We obtained a maximum 30% synaptic weight change and potentiation/depression time scale range from $[-1.5\text{ ms}, 1.1\text{ ms}]$ to $[-32.2\text{ ms}, 24.1\text{ ms}]$. Furthermore, we explore the effect of proposed synapse at the Spiking Neural Network (SNN) level by performing NEST [16]-based simulations of a small SNN implemented with five leaky-integrate-and-fire neurons connected via GNR-based synapses. Our experiments indicated a strong connection between the synaptic plasticity type, i.e., Hebbian and anti-Hebbian, and the number of firing events in the network. Moreover the number of SNN output firing events monotonously varies with respect to the input spikes frequency. For graphene-based Hebbian STDP and spike duration of 20 ms we obtained an SNN behavior relatively similar with the one provided by the SNN with biological STDP.

The proposed design and synaptic plasticity emulation methodology is generic and our simulation results suggest that by changing the GNR shape and contact topologies various synaptic plasticities can be obtained, potentially beyond the six reported cases. Given that the proposed graphene-based synapse has a small footprint (30 nm^2), operates in the hundred-millivolt range, and is versatile from the synaptic behavior point of view, we strongly believe that it can be an outstanding candidate for implementing large-scale energy efficient neuromorphic systems.

The remainder of this article is structured as follows: Section 2 presents the underlying concepts about synapse and synaptic plasticity, and introduces the proposed graphene-based synapse structure. In Section 3, we describe the simulation model for graphene electronic transport properties calculation, and the simulation setup and employed methodology. In Section 4, we present the obtained simulation results, investigate the impact of different spike duration on synaptic plasticity, and explore the effect of synaptic plasticity on neural networks behavior. Section 5 concludes the article.

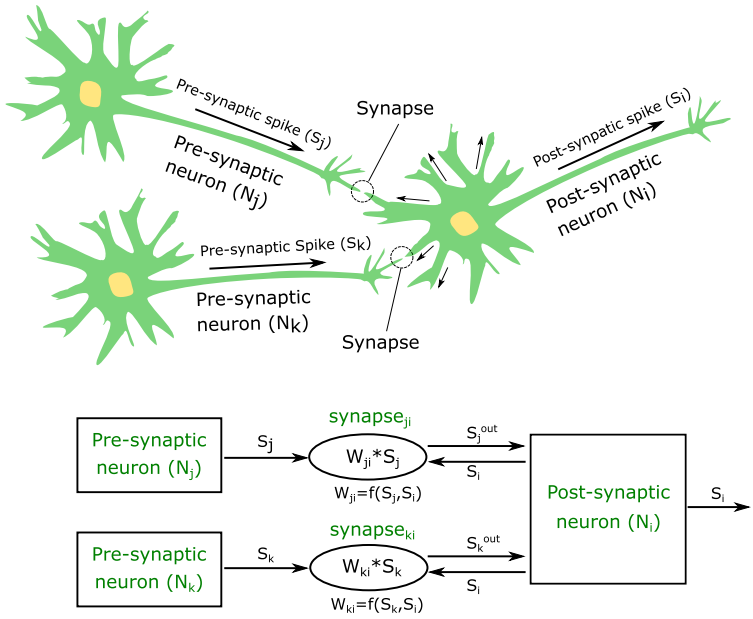

Fig. 1. Synapse-based signal transmission.

2 SYNAPTIC PLASTICITY AND GRAPHENE SYNAPSE

In this section, we present the fundamental concepts underlying synaptic plasticity and then introduce the proposed generic graphene-based synapse.

2.1 Synapse and Synaptic Plasticity

Synapse is the most abundant component in human brain, which serves as the junction connecting two neurons. In order to explain how a synapse affects the information transmission between neurons, a small Neural Network (NN) is depicted in Figure 1. This NN consists of three spiking neurons connected via two synapses. The post-synaptic neuron N_i collects signals (pre-synaptic spikes S_j and S_k) from pre-synaptic neurons N_j and N_k, and when the cumulated signals exceed a certain firing threshold, neuron N_i generates an output signal (post-synaptic spike S_i), which transmits through all its terminations. From the synapse functionality point of view (consider the synapse connecting neurons N_j and N_i), there are: (i) two input signals: pre-synaptic spike S_j, which is output spike of neuron N_j and post-synaptic spike S_i, which is the output spike of neuron N_i, and (ii) one output signal S_j^{out}, which will be transmitted to neuron N_i. The synaptic transmission efficiency (synaptic weight) is a function of the two input spikes, denoted as $W_{ji} = f(S_j, S_i)$. In general, the transmission efficiency is plastic and can either strengthen or weaken the signals transmitted via the synapse. This property is known as synaptic plasticity, which is fundamental synaptic functionality and is believed to be the basis of learning and memory in human brain. There are two types of basic synaptic plasticity: STDP and Long-Term Plasticity (including Long-Term Potentiation (LTP) and Long-Term Depression (LTD)). STDP is a widely used Hebbian synaptic learning rule [9], which suggests that synaptic weight changes according to the relative timing difference between pre-synaptic spike and post-synaptic spike. When the pre-synaptic spike arrives at the synapse shortly before the post-synaptic spike, the synaptic weight increases, and this may lead to a persistent efficiency increase (LTP); otherwise, the synaptic weight

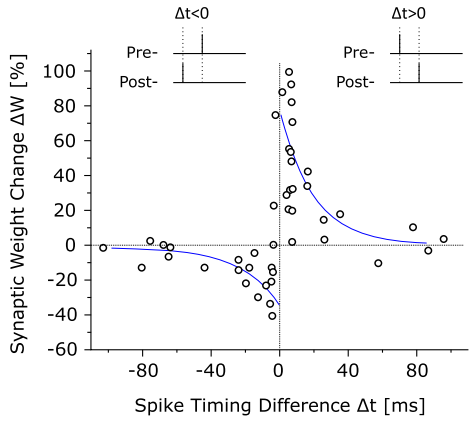

Fig. 2. Biological synapse STDP measured data [7].

decreases, and this may lead to a persistent efficiency decrease (LTD). When the two spikes are very close in time, i.e., very small timing difference, a large synaptic efficiency change occurs. Figure 2 depicts a standard STDP behavior based on biological measured data [7]. ΔW denotes the synaptic weight change and Δt denotes the spike timing difference. We denote by t_{pre} and t_{post}, the arrival time of pre-synaptic spike and post-synaptic spike, respectively. Thus, the spike timing difference is calculated as $\Delta_t = t_{post} - t_{pre}$. Even though the biological synaptic weight change behavior illustrated in Figure 2(a) exhibits stochasticity, a widely accepted STDP interpolating model is as follows:

$$\Delta W(\Delta t) = \begin{cases} A_+ \cdot exp(-\Delta t/\tau_+), & \text{for} \quad \Delta t > 0 \\ -A_- \cdot exp(\Delta t/\tau_-), & \text{for} \quad \Delta t < 0, \end{cases} \tag{1}$$

where A_+ and A_- are parameters affecting the amplitude of synaptic weight change, and τ_+ and τ_- are time constants reflecting the time scale in which the potentiation and depression occurs.

2.2 Graphene-Nanoribbon-Based Synapse

The proposed graphene-based synapse generic structure is illustrated in Figure 3(a) and consists of a single-layer Graphene Nanoribbon (GNR) located on top of an insulating material and a doped substrate serves as back-gate. When a drain-to-source bias voltage $V_d - V_s$ is applied, the GNR constitutes a conduction channel. By shaping the GNR sheet geometry and contact topologies as well as by applying external voltages (e.g., via top-gates and back-gate), the GNR conductance G can be modulated. Figure 3(b) depicts a conductance map (conductance vs. applied voltage) example of the proposed graphene-based synapse generic structure.

From the synaptic behavior point of view, the two top-gates are used for applying synaptic input spikes, e.g., pre-synaptic spike is applied to top-gate-1 and post-synaptic spike to top-gate-2, corresponding to V_{g1} and V_{g2} in Figure 3(a), respectively. The synaptic plasticity is reflected by the induced GNR conductance change, and the output spike current is represented by the drain-to-source current, which corresponds to the synaptic output spike S_j^{out} in Figure 1. A key element in our proposal is the fact that, as experimentally observed, graphene-based device inherently exhibits interface traps [17], which are usually caused by defects in the top-gate oxide, and charges can be trapped from graphene to the interface or released. These trapping and deptrapping phenomena affect the top-gates conductance modulation ability, and as such, when applying an input spike the graphene-based device conductance and output current will depend on the cumulated

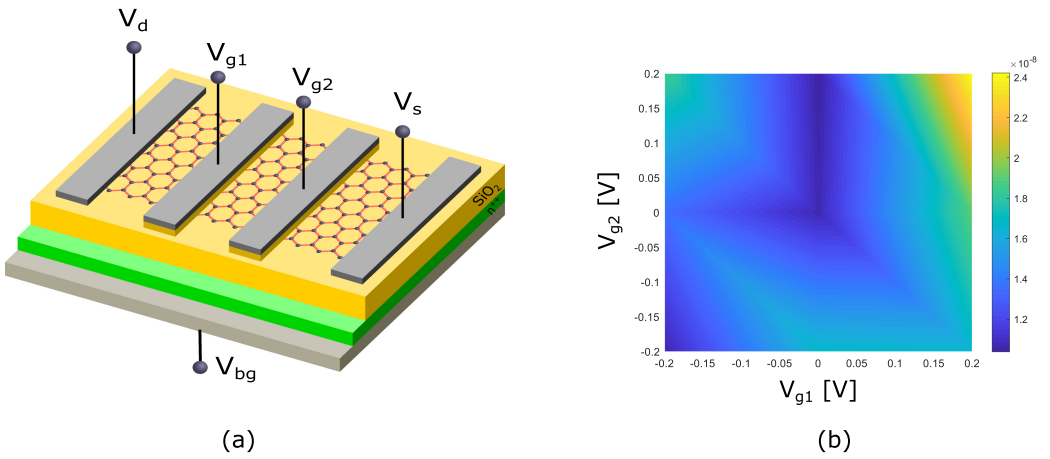

Fig. 3. (a) Graphene-based synapse structure and (b) its conductance map.

previous activities in the artificial synapse. This dependence can be naturally utilized to implement time-varying synaptic plasticity, e.g., STDP, LTP, and LTD. By carving the GNR geometry, the synapse conductance can be modulated such that it reflects a certain functionality. Thus, for every GNR topology a different conductance map can be obtained. As STDP weight change is reflected by the change of the device conductance, with different conductance maps we can have different STDP types. Furthermore, the GNR topology affects as well the trapping mechanism which is fundamental in inducing plasticity.

In Section 4, we demonstrate that by: (i) Shaping the GNR into non-rectangular forms as well as changing the contact topologies, various synaptic plasticities can be obtained, which is not the case for previously proposed rectangular graphene-based synapses [44]; (ii) Changing the back-gate voltage, we can emulate both excitatory and inhibitory synaptic behavior with the same graphene-based device; and (iii) Applying input spikes with different duration, the graphene-based synapse can emulate STDP with varying potentiation/depression time scale without affecting the amplitude of synaptic weight change.

3 SIMULATION FRAMEWORK

In this section, we present the simulation model for computing electronic transport properties of the proposed graphene-based synapse, and describe the simulation setup and employed methodology to emulate the desired synaptic plasticity (the GNR conductance change).

3.1 GNR Electronic Transport Simulation Model

In order to compute the GNR electronic transport properties, we utilize the Tight-Binding approach to represent the system Hamiltonian, the Non-Equilibrium Green Function (NEGF) quantum transport model to solve the Schrödinger equation, and the Landauer-Büttiker formalism to derive the GNR current and conductance [12, 13].

Specifically, the GNR channel is described by a Hamiltonian matrix $H = H_0 + U$, which models the interactions between neighbor carbon atoms via H_0 and external potentials (e.g., top-gate and back-gate voltages) via U. The interaction matrix H_0 is constructed as follows:

$$H_0 = \sum_{i,j} t_{i,j} \left|i\right\rangle \left\langle j\right|, \tag{2}$$

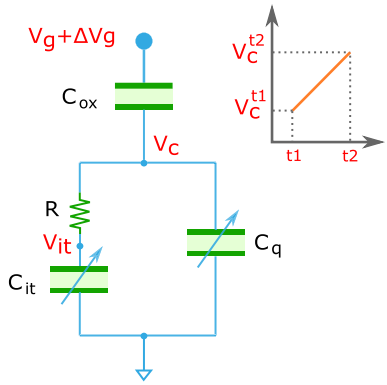

Fig. 4. Equivalent circuit for graphene-based device.

$$\text{where } t_{i,j} = \begin{cases} \tau, & \text{if atoms } i \text{ and } j \text{ are adjacent} \\ 0, & \text{otherwise.} \end{cases} \tag{3}$$

In the simulation, we account for the first nearest-neighbor interaction with $\tau = -2.7eV$. The potential distribution profile U is calculated by solving a 3D Poisson equation self-consistently with finite difference method.

As the interface traps cause an equivalent shift of the gate voltage, denoted as ΔV_g [45], we update the potential distribution profile U with $V_g + \Delta V_g$ when solving the 3D Poisson equation. Figure 4 illustrates the equivalent circuit for the proposed graphene-based device in Figure 3(a), where C_{ox} is the top-gate oxide capacitance, C_q the GNR channel quantum capacitance, and C_{it} the capacitance caused by interface traps. When applying a piece-wise linear V_g (the GNR channel potential changes form V_c^{t1} at time moment $t1$ to V_c^{t2} at time moment $t2$), the interface traps charges can be calculated as:

$$Q_{\text{it}}(t) = C_{\text{it}} \cdot \left[\left(V_c^{t1} + \alpha \cdot t - \alpha \cdot \tau \right) + e^{-\frac{t}{\tau}} \cdot \left(\alpha \cdot \tau - V_c^{t1} + V_{\text{it}}^{t1} \right) \right], \tag{4}$$

where V_{it}^{t1} is the accumulated voltage drop on C_{it} at time moment $t1$, τ is the trapping/detrapping time constant, and α is the V_c ramp slope from $t1$ to $t2$.

Along the GNR transport direction, the source and drain contacts with different electrochemical potential sustain the channel conduction. The interaction between the two contacts can be modeled via the self-energy matrices Σ_1 and Σ_2, respectively. After H and $\Sigma_{1,2}$ are calculated, the transmission function $T(E)$, which models the possibility of one electron being transmitted between the source and drain contacts, can be computed as a function of energy:

$$T(E) = \text{Trace} \left[\Gamma_1 \, G_R \, \Gamma_2 \, G_R^{\dagger} \right], \tag{5}$$

where

$$G_R(E) = [EI - H - \Sigma_1 - \Sigma_2]^{-1}, \tag{6}$$

$$\Gamma_{1,2} = i \left[\Sigma_{1,2} - \Sigma_{1,2}^{\dagger} \right]. \tag{7}$$

The channel current is derived based on the Landauer formula:

$$I = \frac{q}{h} \int_{-\infty}^{+\infty} T(E) \cdot \left(f_0(E - \mu_1) - f_0(E - \mu_2) \right) \, \mathrm{d}E, \tag{8}$$

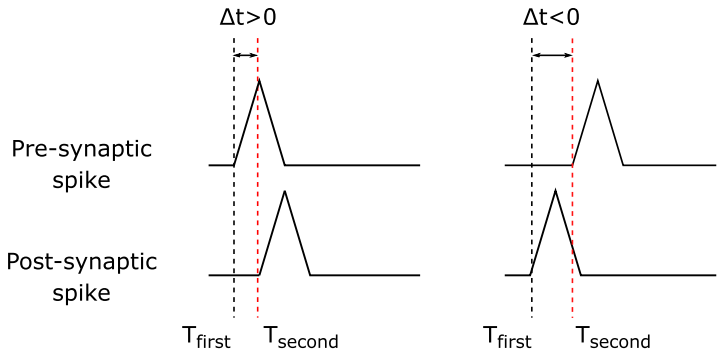

Fig. 5. Spikes timing difference indication.

where $f_0(E)$ denotes the Fermi-Dirac distribution function at temperature T, and $\mu_{1,2}$ represent the source and drain contacts electrochemical potential.

Finally, the GNR conductance can be calculated as:

$$G = \frac{I}{V_d - V_s}. \tag{9}$$

3.2 Simulation Setup and Methodology

In order to emulate STDP behaviors, the pre-synaptic spike and post-synaptic spike are applied to V_{g1} and V_{g2}, respectively. As exemplified in Figure 5, when the pre-synaptic spike arrives before the post-synaptic spike, the spike timing difference $\Delta t > 0$, and $\Delta t < 0$ when they arrive in inverse order. We define T_{first} as the arrival time of the first arriving spike and T_{second} as the arrival time of the second arriving spike. We assume that the applied input spikes lay into 70 mV to 180 mV voltage range and a spike duration of 2 ms. When no spike arrives, the two top-gates are subjected to 70 mV voltage, mimicking the rest potential in biological spike trains. Thus, for the different timing difference of spikes, the voltages applied on two top-gates varies at that specific time moment, causing a time-varying conductance change. Additionally, the long-term plasticity behavior is naturally captured by charge trapping/detrapping phenomena.

In Figure 6, the GNR dimension and contacts topologies are graphically defined. Specifically, W and L represent the GNR sheet width and length, PV_{g1} indicates the distance between top-gate-1 and the drain contact, PV_{g2} indicates the the distance between top-gate-2 and the source contact, while WV_{g1} and WV_{g2} signify the width of top-gate-1 and top-gate-2, respectively. Note that $a = 0.142$ nm denotes the distance between two adjacent carbon atoms. Concerning the traps caused hysteresis, we assume a density of interface traps $2.363 \times 10^{13} cm^{-2}(eV)^{-1}$, and the trapping/detrapping time constant is set to 1 ms [28, 31].

To identify a GNR topology that is able to provide support for a targeted plasticity, we perform a **Design Space Exploration (DSE)** by changing GNR dimension, shape, widths and positions of the two top-gates, and back-gate voltage. For each relevant Δt value, we apply a pair of spike trains (pre-synaptic spike and post-synaptic spike) to the two top-gates and measure the synaptic weight change ΔW (the difference between GNR conductance values at time moments T_{first} and T_{second}, where $T_{\text{second}} - T_{\text{first}} = |\Delta t|$ as illustrated in Figure 5). We assess the resemblance of the obtained synaptic weight change with the desired $\Delta W(\Delta t)$ plasticity and, if this is not satisfactory, we continue DSE by changing the GNR topology parameters.

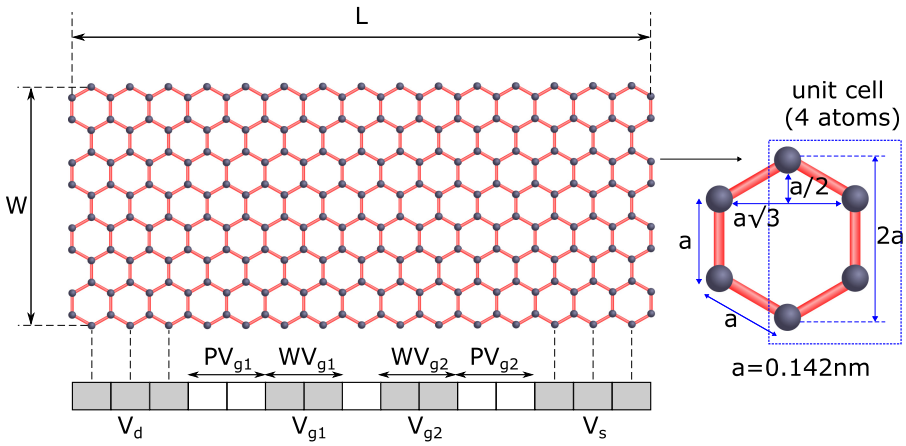

Fig. 6. GNR dimensions and contacts topology.

Table 1. GNR Synapses Topologies

Plasticity Type	W [a]	L [a]	PV_{g1} [a]	WV_{g1} [a]	PV_{g2} [a]	WV_{g2} [a]
Hebbian STDP	23	$25\sqrt{3}$	$9\sqrt{3}$	$3\sqrt{3}$	$2\sqrt{3}$	$6\sqrt{3}$
LTP-biased Hebbian STDP	29	$30\sqrt{3}$	$3\sqrt{3}$	$3\sqrt{3}$	$10\sqrt{3}$	$3\sqrt{3}$
anti-Hebbian STDP	29	$30\sqrt{3}$	$3\sqrt{3}$	$6\sqrt{3}$	$7\sqrt{3}$	$6\sqrt{3}$
LTP-biased anti-Hebbian STDP	23	$25\sqrt{3}$	$9\sqrt{3}$	$3\sqrt{3}$	$2\sqrt{3}$	$3\sqrt{3}$

4 GRAPHENE-BASED SYNAPSES EVALUATION

In this section, we evaluate the capability of the proposed graphene-based synapses to emulate various plasticity types and investigate how input spike duration affects the achieved synaptic plasticity. Finally, we explore the effect of the obtained synaptic plasticity on the behavior of an example spiking neural network.

4.1 Spike-Timing-Dependent Plasticity and Long-Term Plasticity

In order to evaluate the ability of the proposed graphene-based synapse to emulate various plasticity types, we considered four different STDP types underlying balanced and potentiation dominated learning [18, 22]: Hebbian STDP with balanced LTP and LTD (Figure 7(a)), LTP-biased Hebbian STDP (Figure 7(d)), anti-Hebbian STDP with balanced LTP and LTD (Figure 8(a)) and LTP-biased anti-Hebbian STDP (Figure 8(d)). The GNR topologies (overall GNR width and length as well as the widths and positions for two top-gates) for the considered STDP types as determined by means of DSE are summarized in Table 1, where all values are expressed in term of $a = 0.142$ nm, which is the distance between adjacent carbon atoms in a graphene unit cell. The GNR shapes for the four considered cases are depicted in Figures 7(b) and 7(e) and Figures 8(b) and 8(e), which capture their actual dimensions in term of carbon atoms.

Figure 7(b) depicts the obtained GNR shape for Hebbian STDP with balanced LTP and LTD plasticity, with drain-to-source bias voltage $V_d = 0.2$ V and back-gate voltage $V_{back} = 0$ V. The simulated synaptic weight change (conductance change) as presented in Figure 7(c) has a good resemblance with the ideal Hebbian STDP with balanced LTD and LTP behavior trend (Figure 7(a)). One can observe that the range of the obtained synaptic plasticity change is around

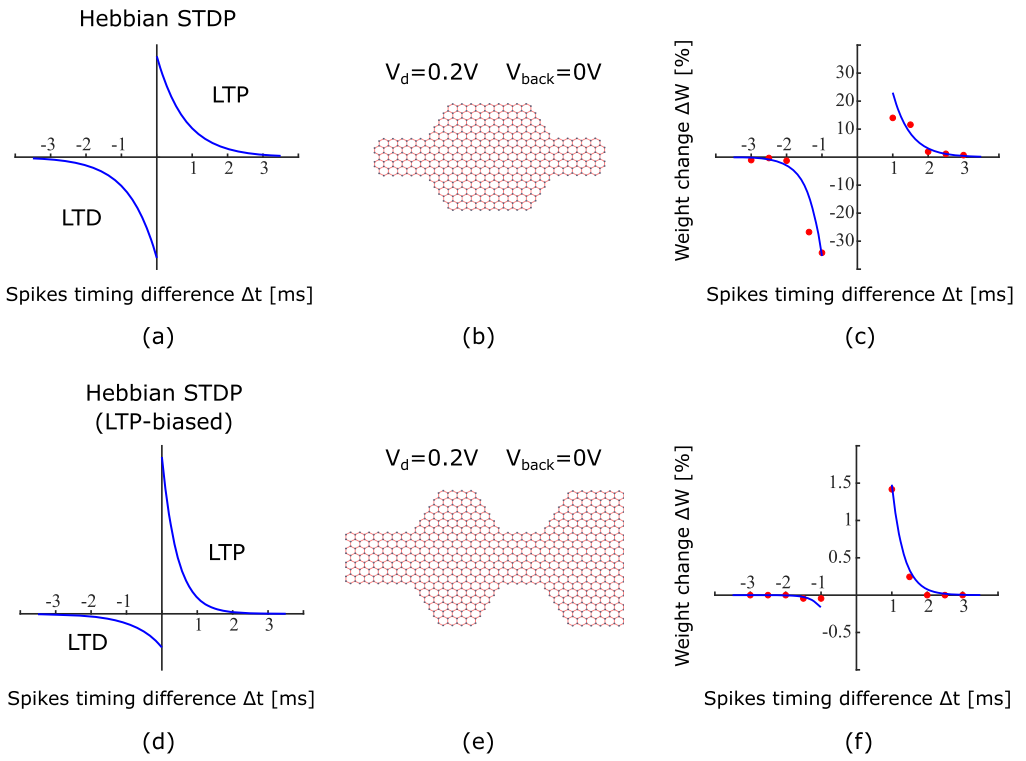

Fig. 7. GNR synapse shapes and obtained plasticity corresponds to Hebbian STDP and LTP-biased Hebbian STDP.

30%. To properly evaluate the obtained synaptic behavior, we define the STDP potentiation and depression time scale (t_+ and t_-, respectively) as the spikes timing difference Δt range in which the corresponding synaptic weight change ΔW is significant, i.e., larger than 0.1%. Thus, when for $t_- < \Delta t < t_+$ the synaptic weight change $|\Delta W| > 0.1\%$. For the simulated Hebbian STDP, we obtain a potentiation time scale $t_+ = 2.6$ ms and depression time scale $t_- = -2.5$ ms, which indicates that the synaptic weight change is tiny when the spikes timing difference is beyond this range([−2.5 ms, 2.6 ms]). We further investigate how different input spikes duration affects the obtained STDP potentiation/depression time scale in 4.2.

Figure 7(e), Figure 8(b), and Figure 8(e) illustrate the obtained GNR shapes for LTP-biased Hebbian STDP, anti-Hebbian STDP with balanced LTP and LTD, and LTP-biased anti-Hebbian STDP, respectively. In all these cases, the drain-to-source bias voltage is $V_d = 0.2$ V and the back-gate voltage $V_{back} = 0$ V. For LTP-biased Hebbian STDP, the simulated synaptic plasticity in Figure 7(f) is temporally asymmetric, and we observe that the amplitude of synaptic weight potentiation is about 3 times larger than synaptic weight depression, which results in a LTP-biased behavior. Compared with the amplitudes obtained for Hebbian STDP with balanced LTP and LTD, the amplitudes in this case are relatively smaller. For obtained anti-Hebbian STDP with balanced LTP and LTD in Figure 8(c), the synaptic weight potentiation amplitude is around 2.5% while the depression amplitude is around 1.5%, which is approximately symmetric and exhibits a good resemblance with the ideal behavior depicted in Figure 8(a). As for the simulated LTP-biased anti-Hebbian STDP in Figure 8(f), the synaptic weight potentiation amplitude is about 30% while the depression amplitude is about 5%, thus exhibiting the obvious LTP-biased behavior. Note that for these

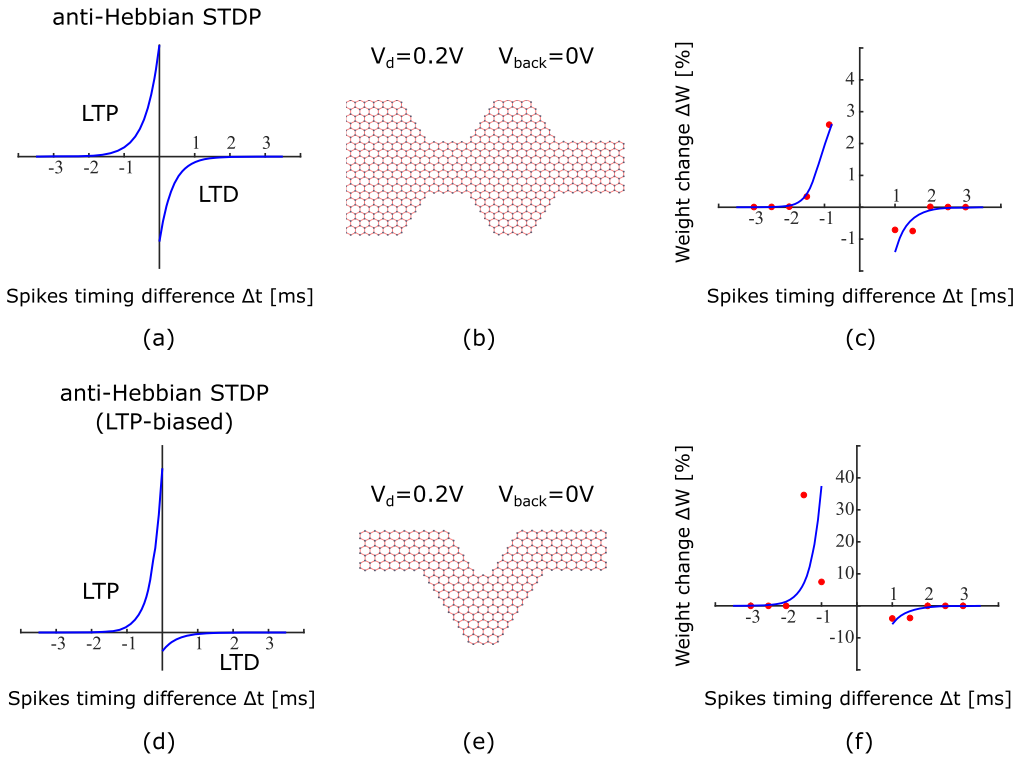

Fig. 8. GNR synapse shapes and obtained plasticity corresponds to anti-Hebbian STDP and LTP-biased anti-Hebbian STDP.

three cases (LTP-biased Hebbian STDP, balanced anti-Hebbian STDP and LTP-biased anti-Hebbian STDP), the obtained plasticity has similar STDP potentiation/depression time scale which is around $[-2\text{ ms}, 2\text{ ms}]$.

A synapse can either exhibit excitatory behavior (i.e., synaptic weight potentiation when the pre-synaptic spike arrives before post-synaptic spike) or inhibitory behavior (i.e., synaptic weight depression when the pre-synaptic spike arrives before post-synaptic spike). To emulate excitatory and inhibitory synaptic behaviors, traditional artificial synapses need two different designs. With the proposed graphene-based synapses, we are able to obtain both excitatory and inhibitory synaptic behaviors with the same graphene-based device by changing the back-gate voltage. For instance, the GNR synapse shape illustrated in Figure 7(b) exhibits an excitatory synaptic behavior. By simply changing the back-gate voltage from 0 V to −0.15 V while keeping the GNR shape, contact topologies, and applied voltages identical, the inhibitory synaptic behavior is obtained as depicted in Figure 9(a). Similarly, the GNR shape depicted in Figure 8(e) exhibits an inhibitory synaptic behavior. By simply changing the back-gate voltage from 0 V to −0.05 V, the corresponding excitatory synaptic behavior is obtained as illustrated in Figure 9(b).

Beside STDP, Long-Term Plasticity (LTP) is a fundamental synaptic functionality, which is believed as the basis of memory in human brain. To obtain LTP, an identical spike is applied to the top-gate-1 consecutively while a constant voltage (the rest potential) is applied to top-gate-2. The applied spikes and the voltage mimicking the rest potential are consistent with the ones used in STDP simulations. In our experiment, we considered the GNR synapse shapes from Figure 7(b) and Figure 8(e) and apply an input spike train consisting of identical spike with inter-spike period 1 ms.

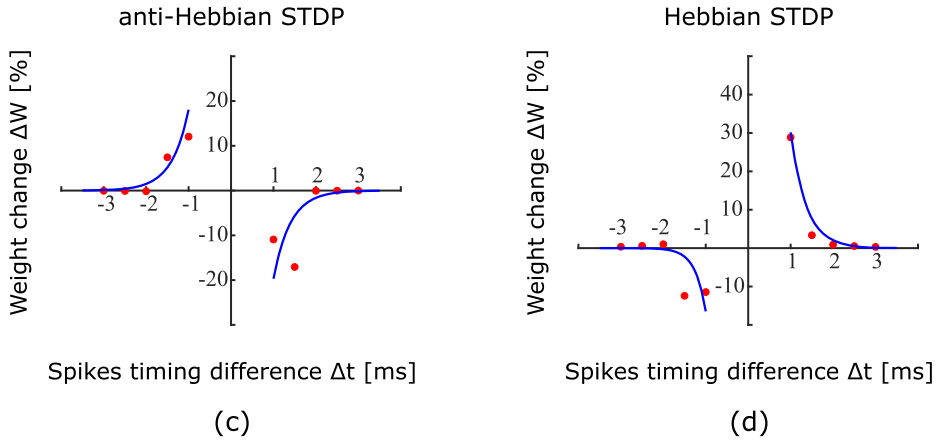

Fig. 9. (a) Corresponding inhibitory synaptic behavior for synapse shape depicted in Figure 7(b), and (b) corresponding excitatory synaptic behavior for synapse shape depicted in Figure 8(e).

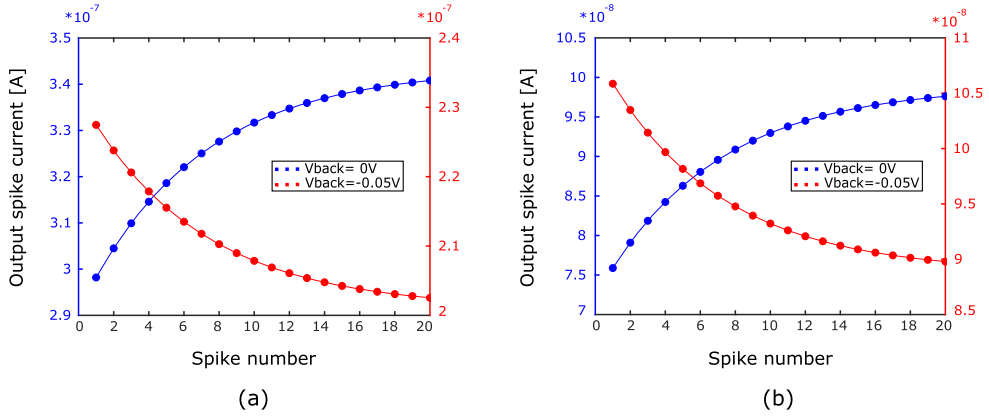

Fig. 10. Output spike current for long-term plasticity. (a) Graphene-based synapse illustrated in Figure 7(b). (b) Graphene-based synapse illustrated in Figure 8(e).

For each spike, we measure the GNR drain to source current, which represents the output spike current generated by the synapse (e.g., S_j^{out} in Figure 1). The long-term potentiation and depression are obtained by properly changing the back-gate voltage for the two GNR synapse shapes, respectively. For both GNR synapse shapes in Figure 7(b) and Figure 8(b), LTP is obtained with back-gate voltage $V_{back} = 0$ V and LTD is obtained with back-gate voltage $V_{back} = -0.05$ V, as illustrated in Figures 10(a) and 10(b), respectively.

Our simulation results demonstrate the capabilities of the proposed artificial synapses to emulate various types of synaptic plasticity. The design and simulation methodology is generic, more synaptic plasticity types can be potentially obtained beyond the aforementioned ones. The proposed graphene-based synapses have small area (max. 30 nm^2) and operate with low operating voltage (0.2 V drain-to-source bias voltage and max. 0.18 V input spike voltage), which are desired properties for large-scale neuromorphic computation systems. To get further into our proposed graphene-based synapses, we investigate in the following subsection how input spikes with different spike duration affect the obtained synaptic plasticity.

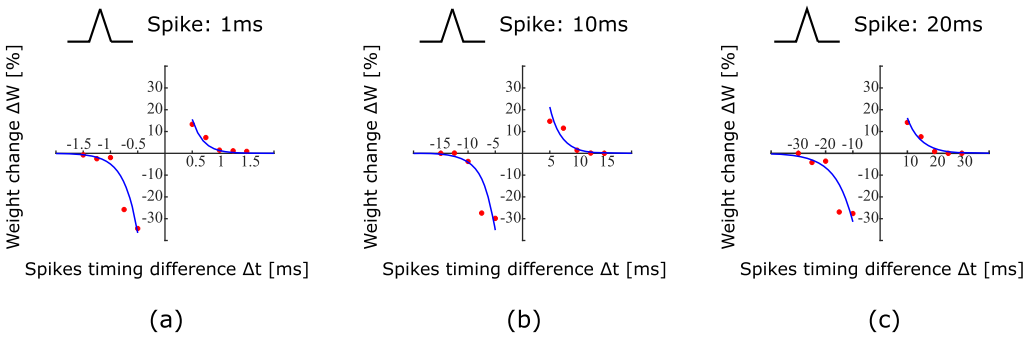

Fig. 11. Simulated STDP with input spike duration (a) 1 ms, (b) 10 ms, and (c) 20 ms.

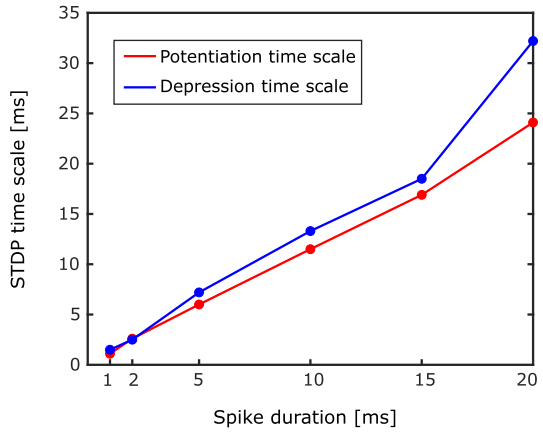

Fig. 12. STDP potentiation and depression time scale vs. input spike duration.

4.2 Spike-Timing-Dependent Plasticity Time Scale Variation

To investigate the effect of varying input spike duration on obtained STDP, we consider the GNR synapse in Figure 7(b) and apply input spike with duration of 1 ms, 10 ms, and 20 ms. For each case, input spikes with the specific duration are applied to the graphene-based synapse and the resulting plasticity are recorded. The GNR geometry, contact topologies, drain-to-source biased voltage and back-gate voltage are identical with the previous STDP simulation. The obtained STDPs are depicted in Figure 11. The simulated STDP in Figure 11(a) corresponds to spike duration 1 ms. The obtained potentiation and depression time scale $t_+ = 1.1$ ms and $t_- = -1.5$ ms, which is smaller than the one obtained with a spike duration of 2 ms. We observe the amplitude of synaptic weight potentiation and depression is around 20% and −30%, respectively, and are almost identical with the ones obtained with a spike duration of 2 ms. The obtained STDP for 10 ms and 20 ms spikes are illustrated in Figures 11(b) and 11(c), respectively. In both the 10 ms and 20 ms cases, the amplitude of the synaptic weight change is around 30%, while the STDP time scale is [−13.3 ms, 11.5 ms] and [−32.2 ms, 24.1 ms], respectively. The simulation results suggest that the input spike duration can affect the obtained STDP potentiation/depression time scale, while having little effect on the synaptic weight change amplitude.

Figure 12 statistically illustrates the relation between the input spike duration and obtained STDP potentiation/depression time scale, when considering [1 ms, 2 ms, 5 ms, 10 ms, 15 ms,

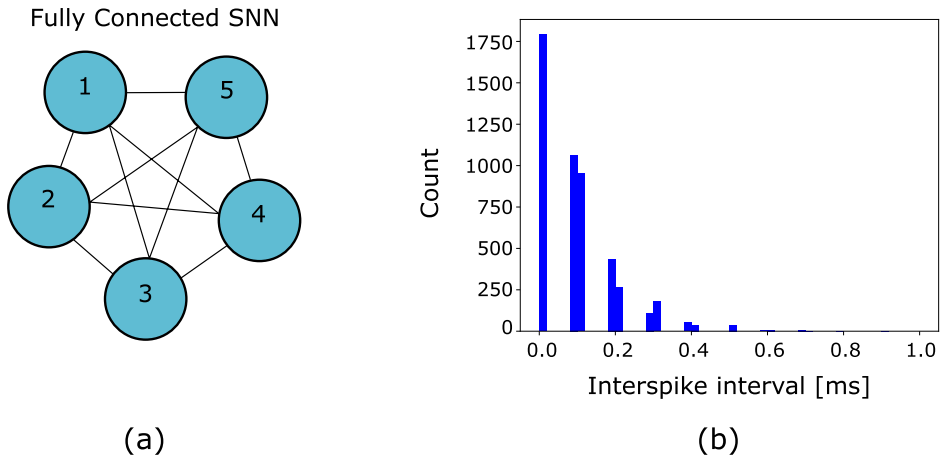

Fig. 13. The simulated fully connected SNN and the inter-spike interval distribution of the input spike train.

20 ms] spikes. One can observe an approximately linear relation between the input spike duration and obtained STDP potentiation/depression time scale. The synaptic weight change amplitudes in all cases are identical. Thus, we conclude that by changing the input spike duration, the proposed synapse can achieve STDP with different potentiation/depression time scale without affecting the amplitudes of synaptic weight change.

4.3 Spiking Neural Network Impact

To get some preliminary understanding on the implication of our proposal at the higher level, we consider a small SNN with GNR-based synapses and simulate its behavior by means of the NEST simulator [16]. As illustrated in Figure 13(a), this SNN has a fully connected network topology, and consists of five leaky-integrate-and-fire neurons connected via synapses. Since, in a given neural network, the spikes are alike, the form of a single spike doesn't carry any information, but the number and timing of spikes matter [21], we concentrate on investigating how the proposed graphene-based synapse affects the SNN's firing behavior. As a thorough analysis of any synaptic plasticity influence on the neural network's behavior is out of the scope of this article, we restrict the investigation to the cases in which the simulated SNN is constructed with the biological synapses (as illustrated in Figure 2) [7] and proposed graphene-based synapses. The plasticity model described in Equation (1) is utilized as standard STDP model in the NEST simulator and we specify synaptic behaviors in SNNs by fitting plasticity data (e.g., biological measured data and simulation results with graphene-based synapses) with the STDP model for different cases. For simplicity, we call the SNN with synaptic behavior specified by biological measured data as SNN with biological STDP, and the SNN with synaptic behavior specified by graphene-based synapses simulation data as SNN with graphene-based STDP (e.g., SNN with graphene-based Hebbian STDP, SNN with graphene-based anti-Hebbian STDP). For the SNN simulation, an input spike train (with spike times sampled from a Poisson distribution) with a firing frequency of 10 kHz is applied to all neurons, and the firing events are recorded. Figure 13 depicts the inter-spike interval distribution of the input spike train. Every simulation is performed with one specific synaptic behavior, while the other settings are keep consistent. The overall simulation time is set to 500 ms.

We consider SNN with biological STDP as baseline and then perform simulations for SNN with graphene-based Hebbian STDP (in Figure 7(c)) and anti-Hebbian STDP (in Figure 8(c)), which

Table 2. SNN Total Output Firing Number

Synaptic Plasticity	Number[#]
STDP with biological STDP	220
Graphene-based Hebbian STDP (2 ms)	820
Graphene-based anti-Hebbian STDP (2 ms)	80
Graphene-based Hebbian STDP (1 ms)	290
Graphene-based Hebbian STDP (20 ms)	200

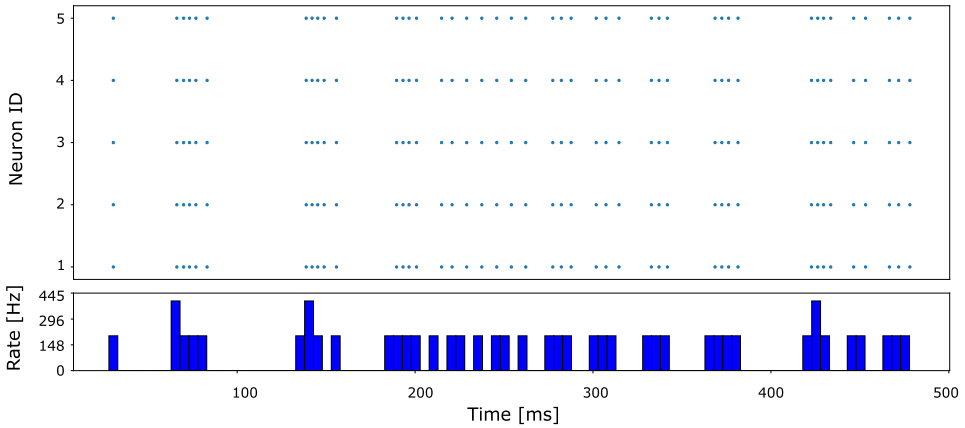

Fig. 14. SNN firing events with biological STDP.

correspond to excitatory and inhibitory synaptic behaviors, respectively. Furthermore, graphene-based Hebbian STDPs obtained with different input spike durations (e.g., spike duration 1 ms in Figure 11(a) and spike duration 20 ms in Figure 11(c)) are also utilized to perform the simulation. Table 2 summarizes the obtained total number of firing events for all cases. The graphene-based synaptic plasticity types are indicated by the applied spike duration in previous GNR simulations, e.g., graphene-based Hebbian STDP (2 ms) indicates the corresponding plasticity obtained with input spike duration of 2 ms.

Figure 14 illustrates the simulation results for SNN with biological STDP. The top panel shows a raster plot for firing events belonging to the five neurons. Each dot in the plot indicates the occurrence time of one firing event and all dots in the same row belong to the same neuron. The histogram plot in the bottom panel represents the SNN firing rate at each time moment. As the simulated SNN has a fully connected topology and inputs are applied to all neurons, the firing events for all neurons are identical, which can be observed through the same firing events distribution for the five neurons. As for the firing rate in the histogram plot it exhibits a sparse distribution and there is no obvious tendency to increase or decrease. The total firing events number in this case is 220.

Figure 15(a) depicts the simulation results for SNN with graphene-based Hebbian STDP (2 ms). One can observe a dramatic increase of the firing rate during the first 100 ms and then the SNN keeps a relatively high firing rate until the end. The total firing events number is 820, which is 3.7 times larger than the one obtained in SNN with biological STDP, which suggests that the graphene-based Hebbian STDP is able to exhibit a significant strengthening effect on the SNN's firing events.

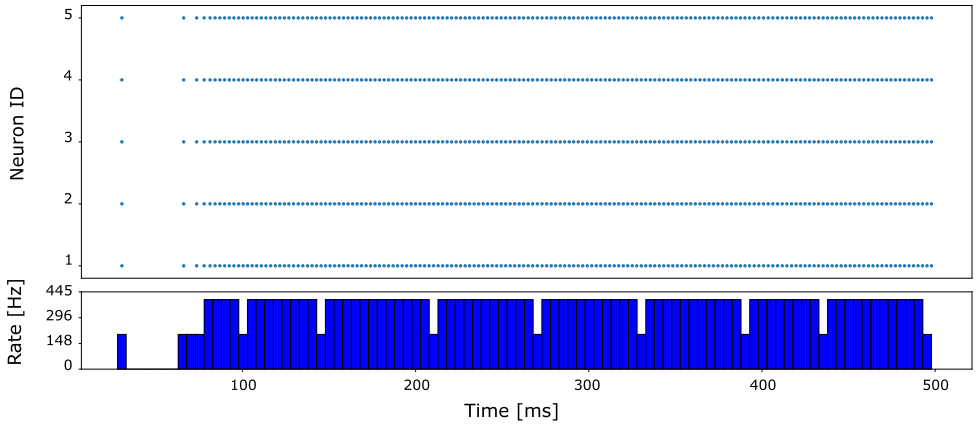

(a) SNN with graphene-based Hebbian STDP (2ms)

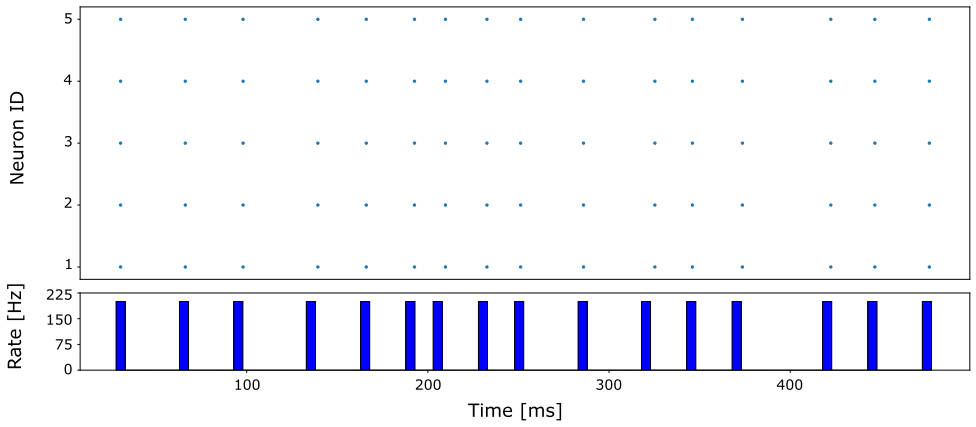

(b) SNN with graphene-based anti-Hebbian STDP (2ms)

Fig. 15. SNN firing events with proposed Hebbian STDP and anti-Hebbian STDP.

The simulation results for SNN with graphene-based anti-Hebbian STDP (2 ms) is illustrated in Figure 15(b). One can observe that the general firing rate is smaller than the aforementioned two SNN simulations, and it exhibits a sparser firing events distribution. The total firing events number is 80, which suggests that proposed graphene-based anti-Hebbian synapse can properly emulate inhibitory synaptic behavior and suppress the SNN's firing events.

To evaluate the implications of the spike length we perform simulations also for SNNs with graphene-based Hebbian STDP (1 ms) and with graphene-based Hebbian STDP (20 ms), which results are illustrated in Figures 16(a) and 16(b), respectively. We observe that, for the SNN with graphene-based Hebbian STDP (1 ms), there is a gradual increase of the firing rate, and the total firing events number is 290. Compared with SNN with biological STDP, this graphene-based synapse can exhibit strengthening effect, but is weaker than the one observed in Figure 15(a). As for the SNN with graphene-based Hebbian STDP 20 ms, the firing events have sparse distribution and don't exhibit any strengthening or weakening tendency, which is similar to the response of the SNN with biological STDP. As presented in 4.2, graphene-based Hebbian STDPs with spike duration (1 ms) and 20 ms have identical synaptic weight change amplitude and the potentiation/depression time scales are different. The firing events observed in these two

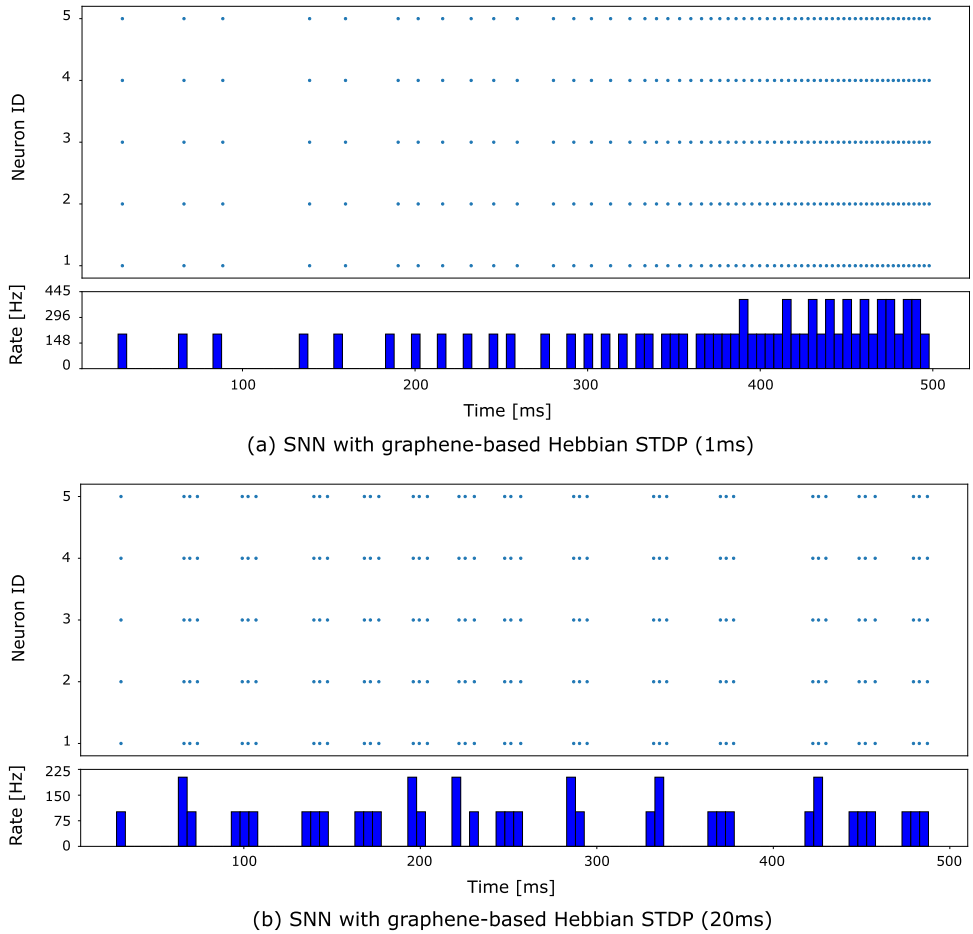

Fig. 16. SNN firing events with proposed Hebbian STDP obtained with different spike duration.

cases indicate that the potential/depression time scale has an obvious influence on the SNN's behaviors.

In order to investigate how input spike frequency affects the SNN output firing events, we consider three different STDP types, i.e., biological STDP, graphene-based Hebbian STDP (2 ms), and graphene-based Hebbian STDP (20 ms), and vary the SNN input spike frequency from 10 kHz to 30 kHz. Simulation results are presented in Figure 17 and indicate that the number of SNN output firing events for all three STDP cases monotonously varies with respect to the input spikes frequency. Specifically, we observe: (i) an increase of 13% in the SNN output firing rate for the graphene-based Hebbian STDP (2 ms) and (ii) $\approx 2\times$ increases for both biological STDP and graphene-based Hebbian STDP (20 ms)). Furthermore, we notice a close resemblance between the SNN firing rates for the biological and the Hebbian 20 ms STDP cases for all input spike frequencies, which is consistent with the results reported in aforementioned simulations.

4.4 Synapses Implementations in Current Technologies

To have a better view of the synapse designs landscape, and investigate in this context the potential of using graphene-based synapses for large-scale neuromorphic systems, we consider different

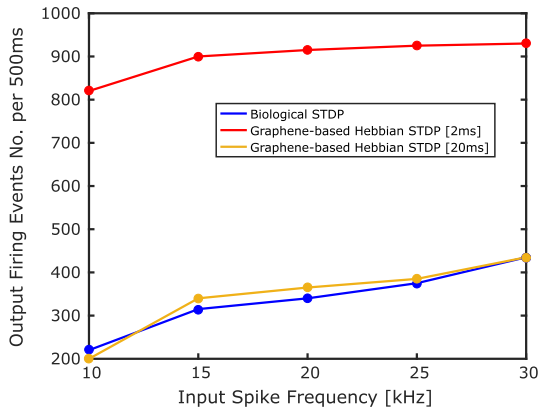

Fig. 17. SNN output firing events number with different input spike frequencies.

technologies, i.e., CMOS, memristor, and evaluate comparatively the synaptic implementations summarized in Table 3.

From the large-scale implementations' suitability point of view, we look at the synapse footprint and operating voltage. Area-wise, the synapse designs based on emerging technologies, i.e., memristors [24, 46] and graphene [41], have generally compact implementations, and are thus better equipped than CMOS-based counterparts [23, 34] for a high density of integration. The proposed GNR synapse design has a 30 nm^2 footprint, which is 2 orders and 5 orders of magnitude smaller than memristor and CMOS designs, respectively. Furthermore, our GNR synapse operates at low voltage (0.2 V), at least 5× smaller than memristor- and CMOS-based counterparts, which is essential when striving for brain-akin energy efficiency envelopes. From the functionality point of view, to emulate abundant enough neural network dynamics, synapse designs require flexibility for mimicking an enriched repertoire of synaptic plasticities. Memristor and CMOS synapse designs, in order to adapt to different STDP types, rely on external control signals and additional circuitry that generates for each STDP type, input spikes with the required shapes [23, 40]. Unlike the aforementioned adaptation approaches, the proposed GNR-based synapse structure can accommodate various STDP types within a single graphene-based device simply by carving a different GNR geometry for each STDP type. So, for different plasticity types, we have different devices, i.e., the same single graphene-based synapse structure but with another GNR geometry. The fact that the STDP adaptation ability is obtained with the same input spike shapes for all STDP types and that the entire synaptic functionality can be encapsulated within a single device, makes the proposed GNR-based synapse structure a versatile modular plug-in component for neural network implementations. When compared to existing graphene-based synapse designs [41, 44], our proposal outperforms its counterparts by requiring 30× to 5 orders of magnitude less area and by straightforward emulation of different plasticity types. The comparison clearly indicates that the proposed GNR-based synapse, by its low real-estate requirements, small operating voltage, as well as adaptation versatility to different synaptic plasticity types, exhibits a high potential for large-scale and functionally diverse neuromorphic computing platform implementations.

5 CONCLUSIONS

In this article, we proposed a generic non-rectangular Graphene-Nanoribbon (GNR)-based synapse. We demonstrated that by properly changing the GNR shape and contact topologies, and applying external voltages, the proposed graphene-based synapse is capable of mimicking various synaptic plasticity types. Moreover, the same graphene-based synapse can emulate both excitatory

Table 3. Synapse Implementations with Different Technologies

Synapse Type	Operating Voltage	Area	STDP type Adaptation
Biological [7]	Spike: $[-40, 70]$mV	-	-
CMOS [23]	Spike: 1 V	-	Yes
CMOS [34]	Supply:1 V	$\approx 1.3 \times 10^7 \text{nm}^2$	No
Memristor [24]	Spike: $[-1, 1]$V	-	No
Memristor [46]	Spike: $[-5, 1.5]$V	$\approx 1.0 \times 10^4 \text{nm}^2$	No
Graphene [44]	Supply:0.1 V, Spike: 2 V	$\approx 9.0 \times 10^6 \text{nm}^2$	No
Graphene [41]	Supply:0.1 V	$\approx 9.0 \times 10^2 \text{nm}^2$	No
Proposed Design	Supply:0.2 V, Spike: 0.18 V	$\approx 3.0 \times 10^1 \text{nm}^2$	Yes

and inhibitory synaptic plasticity by simply changing its back-gate voltage. We successfully emulated two fundamental synaptic functionalities: Spike-Timing-Dependent Plasticity (STDP) and Long-Term Plasticity (LTP), including long-term potentiation and long-term depression, which are foundational for human brain learning and remembering capabilities. Given that we relied on a generic methodology to identify the appropriate GNR topology for a desired synaptic plasticity our proposal is by no means restricted to the four STDP types and two LTP types considered in this article. We also investigated the relation between the input spike duration and the synaptic plasticity potentiation/depression time scale. the simulation results suggested that the proposed graphene-based synapses can emulate STDPs with various potentiation/depression time scales without changing the obtained synaptic weight change amplitude. This property makes the proposed synapse versatile in emulating various plasticity types suitable for different application scenarios. For the simulated synaptic plasticity cases, we obtained a maximum 30% synaptic weight change and potentiation/depression time scale ranging from $[-1.5$ ms, 1.1 ms$]$ to $[-32.2$ ms, 24.1 ms$]$. Furthermore, we explored the effect of proposed synapse at the Spiking Neural Network (SNN) level by performing NEST-based simulations of a small SNN implemented with five leaky-integrate-and-fire neurons connected via GNR-based synapses. Our experiments indicated a strong connection between the synaptic plasticity type, i.e., Hebbian and anti-Hebbian, and the number of firing events in the network. Moreover the number of SNN output firing events monotonously varies with respect to the input spikes frequency. For graphene-based Hebbian STDP and spike duration of 20 ms, we obtained an SNN behavior relatively similar with the one provided by the SNN with biological STDP. The proposed graphene-based synapse has a small area (30 nm^2), operates in the 100 mV bias and input range, and can emulate various plasticity types, which is making it a very promising candidate for large-scale energy-efficient neuromorphic system implementations.

REFERENCES

[1] Filipp Akopyan, Jun Sawada, Andrew Cassidy, Rodrigo Alvarez-Icaza, John Arthur, Paul Merolla, Nabil Imam, Yutaka Nakamura, Pallab Datta, Gi-Joon Nam, Brian Taba, Michael Beakes, Bernard Brezzo, Jente B. Kuang, Rajit Manohar, William P. Risk, Bryan Jackson, and Dharmendra S. Modha. 2015. Truenorth: Design and tool flow of a 65 mw 1 million neuron programmable neurosynaptic chip. *IEEE Transactions on Computer-Aided Design of Integrated Circuits and Systems* 34, 10 (2015), 1537–1557.

[2] Matthew J. Allen, Vincent C. Tung, and Richard B. Kaner. 2009. Honeycomb carbon: A review of graphene. *Chemical Reviews* 110, 1 (2009), 132–145.

[3] Phaedon Avouris and Christos Dimitrakopoulos. 2012. Graphene: Synthesis and applications. *Materials Today* 15, 3 (2012), 86–97.

[4] Yunus Babacan and Fırat Kaçar. 2017. Memristor emulator with spike-timing-dependent-plasticity. *AEU-International Journal of Electronics and Communications* 73 (2017), 16–22.
[5] Mark F. Bear and Robert C. Malenka. 1994. Synaptic plasticity: LTP and LTD. *Current Opinion in Neurobiology* 4, 3 (1994), 389–399.
[6] Ben Varkey Benjamin, Peiran Gao, Emmett McQuinn, Swadesh Choudhary, Anand R. Chandrasekaran, Jean-Marie Bussat, Rodrigo Alvarez-Icaza, John V. Arthur, Paul A. Merolla, and Kwabena Boahen. 2014. Neurogrid: A mixed-analog-digital multichip system for large-scale neural simulations. *Proc. IEEE* 102, 5 (2014), 699–716.
[7] Guo-qiang Bi and Mu-ming Poo. 1998. Synaptic modifications in cultured hippocampal neurons: Dependence on spike timing, synaptic strength, and postsynaptic cell type. *Journal of Neuroscience* 18, 24 (1998), 10464–10472.
[8] Kwabena Boahen. 2005. Neuromorphic microchips. *Scientific American* 292, 5 (2005), 56–63.
[9] Natalia Caporale and Yang Dan. 2008. Spike timing-dependent plasticity: A Hebbian learning rule. *Annual Review of Neuroscience* 31 (2008), 25–46.
[10] Ami Citri and Robert C. Malenka. 2008. Synaptic plasticity: Multiple forms, functions, and mechanisms. *Neuropsychopharmacology* 33, 1 (2008), 18–41.
[11] Yang Dan and Mu-ming Poo. 2004. Spike timing-dependent plasticity of neural circuits. *Neuron* 44, 1 (2004), 23–30.
[12] Supriyo Datta. 2000. Nanoscale device modeling: The Green's function method. *Superlattices and Microstructures* 28, 4 (2000), 253–278.
[13] Supriyo Datta. 2005. *Quantum Transport: Atom to Transistor*. Cambridge University Press.
[14] Mike Davies, Narayan Srinivasa, Tsung-Han Lin, Gautham Chinya, Yongqiang Cao, Sri Harsha Choday, Georgios Dimou, Prasad Joshi, Nabil Imam, Shweta Jain, Yuyun Liao, Chit-Kwan Lin, Andrew Lines, Ruokun Liu, Deepak Mathaikutty, Steve McCoy, Arnab Paul, Jonathan Tse, Guruguhanathan, Venkataramanan, Yi-Hsin Weng, Andreas Wild, Yoonseok Yang, and Hong Wang. 2018. Loihi: A neuromorphic manycore processor with on-chip learning. *IEEE Micro* 38, 1 (2018), 82–99.
[15] Peter U. Diehl and Matthew Cook. 2015. Unsupervised learning of digit recognition using spike-timing-dependent plasticity. *Frontiers in Computational Neuroscience* 9 (2015), 99.
[16] Tanguy Fardet, Stine Brekke Vennemo, Jessica Mitchell, Håkon Mørk, Steffen Graber, Jan Hahne, Sebastian Spreizer, Rajalekshmi Deepu, Guido Trensch, Philipp Weidel, Jakob Jordan, Jochen Martin Eppler, Dennis Terhorst, Abigail Morrison, Charl Linssen, Alberto Antonietti, Kael Dai, Alexey Serenko, Binghuang Cai, Piotr Kubaj, Robin Gutzen, Hanjia Jiang, Itaru Kitayama, Björn Jürgens, and Hans Ekkehard Plesser. 2020. NEST 2.20.0. https://doi.org/10.5281/zenodo.3605514
[17] Andrea C. Ferrari, Francesco Bonaccorso, Vladimir Fal'Ko, Konstantin S. Novoselov, Stephan Roche, Peter Bøggild, Stefano Borini, Frank H. L. Koppens, Vincenzo Palermo, Nicola Pugno, José A. Garrido, Roman Sordan, Alberto Bianco, Laura Ballerini, Maurizio Prato, Elefterios Lidorikis, Jani Kivioja, Claudio Marinelli, Tapani Ryhänen, Alberto Morpurgo, Jonathan N. Coleman, Valeria Nicolosi, Luigi Colombo, Albert Fert, Mar Garcia-Hernandez, Adrian Bachtold, Grégory F. Schneider, Francisco Guinea, Cees Dekker, Matteo Barbone, Zhipei Sun, Costas Galiotis, Alexander N. Grigorenko, Gerasimos Konstantatos, Andras Kis, Mikhail Katsnelson, Lieven Vandersypen, Annick Loiseau, Vittorio Morandi, Daniel Neumaier, Emanuele Treossi, Vittorio Pellegrini, Marco Polini, Alessandro Tredicucci, Gareth M. Williams, Byung Hee Hong, Jong-Hyun Ahn, Jong Min Kim, Herbert Zirath, Bart J. van Wees, Herre van der Zant, Luigi Occhipinti, Andrea Di Matteo, Ian A. Kinloch, Thomas Seyller, Etienne Quesnel, Xinliang Feng, Ken Teo, Nalin Rupesinghe, Pertti Hakonen, Simon R. T. Neil, Quentin Tannock, Tomas Löfwander, and Jari Kinaret. 2015. Science and technology roadmap for graphene, related two-dimensional crystals, and hybrid systems. *Nanoscale* 7, 11 (2015), 4598–4810.
[18] Robert C. Froemke, Mu-ming Poo, and Yang Dan. 2005. Spike-timing-dependent synaptic plasticity depends on dendritic location. *Nature* 434, 7030 (2005), 221.
[19] Steve B. Furber, David R. Lester, Luis A. Plana, Jim D. Garside, Eustace Painkras, Steve Temple, and Andrew D. Brown. 2013. Overview of the spinnaker system architecture. *IEEE Trans. Comput.* 62, 12 (2013), 2454–2467.
[20] Wulfram Gerstner and Werner M. Kistler. 2002. *Spiking Neuron Models: Single Neurons, Populations, Plasticity*. Cambridge University Press.
[21] Wulfram Gerstner, Werner M. Kistler, Richard Naud, and Liam Paninski. 2014. *Neuronal Dynamics: From Single Neurons to Networks and Models of Cognition*. Cambridge University Press.
[22] Christoph Hartmann, Daniel C. Miner, and Jochen Triesch. 2016. Precise synaptic efficacy alignment suggests potentiation dominated learning. *Frontiers in Neural Circuits* 9 (2016), 90.
[23] Chongyang Huan, Yuan Wang, Xiaoxin Cui, and Xing Zhang. 2020. A reconfigurable mixed signal CMOS design for multiple STDP learning rules. In *IEEE 3rd International Conference on Electronics Technology (ICET)*. 639–643.
[24] Weichuan Huang, Yue-Wen Fang, Yuewei Yin, Bobo Tian, Wenbo Zhao, Chuangming Hou, Chao Ma, Qi Li, Evgeny Y. Tsymbal, Chun-Gang Duan, and Xiaoguang Li. 2018. Solid-state synapse based on magnetoelectrically coupled memristor. *ACS Applied Materials & Interfaces* 10, 6 (2018), 5649–5656.

[25] Eric Hunsberger and Chris Eliasmith. 2015. Spiking deep networks with LIF neurons. (2015). arXiv:1510.08829 http://arxiv.org/abs/1510.08829.
[26] Yande Jiang, Nicoleta Cucu Laurenciu, He Wang, and Sorin Dan Cotofana. 2019. Graphene nanoribbon based complementary logic gates and circuits. *IEEE Transactions on Nanotechnology* 18 (2019), 287–298.
[27] Sung Hyun Jo, Ting Chang, Idongesit Ebong, Bhavitavya B. Bhadviya, Pinaki Mazumder, and Wei Lu. 2010. Nanoscale memristor device as synapse in neuromorphic systems. *Nano Letters* 10, 4 (2010), 1297–1301.
[28] Ukjin Jung, Yun Ji Kim, Yonghun Kim, Young Gon Lee, and Byoung Hun Lee. 2015. Extraction of the interface state density of top-gate graphene field-effect transistors. *IEEE Electron Device Letters* 36, 4 (2015), 408–410.
[29] Saeed Reza Kheradpisheh, Mohammad Ganjtabesh, Simon J. Thorpe, and Timothée Masquelier. 2018. STDP-based spiking deep convolutional neural networks for object recognition. *Neural Networks* 99 (2018), 56–67.
[30] Chankyu Lee, Syed Shakib Sarwar, and Kaushik Roy. 2019. Enabling spike-based backpropagation in state-of-the-art deep neural network architectures. (2019). arXiv:1903.06379 http://arxiv.org/abs/1903.06379.
[31] Young Gon Lee, Chang Goo Kang, Uk Jin Jung, Jin Ju Kim, Hyeon Jun Hwang, Hyun-Jong Chung, Sunae Seo, Rino Choi, and Byoung Hun Lee. 2011. Fast transient charging at the graphene/SiO 2 interface causing hysteretic device characteristics. *Applied Physics Letters* 98, 18 (2011), 183508.
[32] Bernabé Linares-Barranco and Teresa Serrano-Gotarredona. 2009. Memristance can explain spike-time-dependent-plasticity in neural synapses. *Nature Precedings* (2009), 1–1.
[33] Guanxiong Liu, Sonia Ahsan, Alexander G. Khitun, Roger K. Lake, and Alexander A. Balandin. 2013. Graphene-based non-Boolean logic circuits. *Journal of Applied Physics* 114, 15 (2013), 154310.
[34] Christian Mayr, Johannes Partzsch, Marko Noack, Stefan Hänzsche, Stefan Scholze, Sebastian Höppner, Georg Ellguth, and Rene Schüffny. 2015. A biological-realtime neuromorphic system in 28 nm CMOS using low-leakage switched capacitor circuits. *IEEE Transactions on Biomedical Circuits and Systems* 10, 1 (2015), 243–254.
[35] Carver Mead. 1990. Neuromorphic electronic systems. *Proc. IEEE* 78, 10 (1990), 1629–1636.
[36] Paul A. Merolla, John V. Arthur, Rodrigo Alvarez-Icaza, Andrew S. Cassidy, Jun Sawada, Filipp Akopyan, Bryan L. Jackson, Nabil Imam, Chen Guo, Yutaka Nakamura, Bernard Brezzo, Ivan Vo, Steven K. Esser, Rathinakumar Appuswamy, Brian Taba, Arnon Amir, Myron D. Flickner, William P. Risk, Rajit Manohar, and Dharmendra S. Modha. 2014. A million spiking-neuron integrated circuit with a scalable communication network and interface. *Science* 345, 6197 (2014), 668–673.
[37] Ning Qiao, Hesham Mostafa, Federico Corradi, Marc Osswald, Fabio Stefanini, Dora Sumislawska, and Giacomo Indiveri. 2015. A reconfigurable on-line learning spiking neuromorphic processor comprising 256 neurons and 128K synapses. *Frontiers in Neuroscience* 9 (2015), 141.
[38] Sylvain Saïghi, Christian G. Mayr, Teresa Serrano-Gotarredona, Heidemarie Schmidt, Gwendal Lecerf, Jean Tomas, Julie Grollier, Sören Boyn, Adrien F. Vincent, Damien Querlioz, Selina La Barbera, Fabien Alibart, Dominique Vuillaume, Olivier Bichler, Christian Gamrat, and Bernabé Linares-Barranco. 2015. Plasticity in memristive devices for spiking neural networks. *Frontiers in Neuroscience* 9 (2015), 51.
[39] Johannes Schemmel, Daniel Briiderle, Andreas Griibl, Matthias Hock, Karlheinz Meier, and Sebastian Millner. 2010. A wafer-scale neuromorphic hardware system for large-scale neural modeling. In *IEEE International Symposium on Circuits and Systems*. 1947–1950.
[40] Teresa Serrano-Gotarredona, Timothée Masquelier, Themistoklis Prodromakis, Giacomo Indiveri, and Bernabe Linares-Barranco. 2013. STDP and STDP variations with memristors for spiking neuromorphic learning systems. *Frontiers in Neuroscience* 7 (2013), 2.
[41] Mohammad Taghi Sharbati, Yanhao Du, Jorge Torres, Nolan D. Ardolino, Minhee Yun, and Feng Xiong. 2018. Low-power, electrochemically tunable graphene synapses for neuromorphic computing. *Advanced Materials* 30, 36 (2018), 1802353.
[42] Roman Sordan, Floriano Traversi, and Valeria Russo. 2009. Logic gates with a single graphene transistor. *Applied Physics Letters* 94, 7 (2009), 51.
[43] Dmitri B. Strukov, Gregory S. Snider, Duncan R. Stewart, and R. Stanley Williams. 2008. The missing memristor found. *Nature* 453, 7191 (2008), 80.
[44] He Tian, Wentian Mi, Xue-Feng Wang, Haiming Zhao, Qian-Yi Xie, Cheng Li, Yu-Xing Li, Yi Yang, and Tian-Ling Ren. 2015. Graphene dynamic synapse with modulatable plasticity. *Nano Letters* 15, 12 (2015), 8013–8019.
[45] He Wang, Nicoleta Cucu Laurenciu, Yande Jiang, and S. D. Cotofana. 2019. Atomistic-level hysteresis-aware graphene structures electron transport model. In *IEEE International Symposium on Circuits and Systems (ISCAS)*. 1–5.
[46] Zhongrui Wang, Saumil Joshi, Sergey E. Savel'ev, Hao Jiang, Rivu Midya, Peng Lin, Miao Hu, Ning Ge, John Paul Strachan, Zhiyong Li, Qing Wu, Mark Barnell, Geng-Lin Li, Huolin L. Xin, R. Stanley Williams, Qiangfei Xia, and J. Joshua Yang. 2017. Memristors with diffusive dynamics as synaptic emulators for neuromorphic computing. *Nature Materials* 16, 1 (2017), 101–108.

Received May 2020; revised December 2020; accepted January 2021